Fabrication of graphene oxide-modified self-healing microcapsules for Cardanol-based epoxy anti-corrosion coatings

Wu, Wentao; Chu, Liangyong; Garcia, Santiago J.; van der Zwaag, Sybrand; Li, Ming; Shen, Liming; Bao, Ningzhong

DOI
10.1016/j.porgcoat.2023.107777

Publication date
2023

Document Version
Final published version

Published in
Progress in Organic Coatings

Progress in Organic Coatings 183 (2023) 107777

Contents lists available at ScienceDirect

Progress in Organic Coatings

journal homepage: www.elsevier.com/locate/porgcoat

Fabrication of graphene oxide-modified self-healing microcapsules for Cardanol-based epoxy anti-corrosion coatings

Wentao Wu [a], Liangyong Chu [a,*], Santiago J. Garcia [b,*], Sybrand van der Zwaag [b], Ming Li [c], Liming Shen [a,*], Ningzhong Bao [a]

[a] State Key Laboratory of Materials-Oriented Chemical Engineering, College of Chemical Engineering, Nanjing Tech University, Nanjing, Jiangsu 210009, PR China
[b] Department of Aerospace Structures and Materials, Faculty of Aerospace Engineering, Delft University of Technology, 2629HS Delft, the Netherlands
[c] College of Biotechnology and Pharmaceutical Engineering, Nanjing Tech University, Nanjing, Jiangsu 210009, PR China

ARTICLE INFO

Keywords:
Modified-GO
Microcapsules
Cardanol-based coating
Corrosion resistance
Self-healing

ABSTRACT

In this paper, graphene oxide (GO) modified microcapsules have been developed for use in self-healing Cardanol-based epoxy anti-corrosion coatings on steel substrates. The microcapsules had a polymethyl methacrylate (PMMA) shell, covered with aminated GO flakes and contained either of the two complementary healing agents mixed with nanosized GO flakes. One set of capsules contained epoxidized nanosized GO and Cardanol-based epoxy resin, while the other contained aminated nanosized GO and Cardanol-based amine curing agent. The microcapsules had a narrow size distribution with a peak value of 4 μm. The Cardanol-based coatings containing various fractions of up to 20 wt% microcapsules in their stoichiometric ratio showed excellent anti-corrosion and self-healing properties. FT-IR, XPS, AFM, and Raman spectroscopy were used to characterize the size and chemical composition of the GO. Optical microscopy and SEM were used for morphological characterization. Double cantilever test upon bulk samples showed an excellent load transfer across the fracture plane after only 1 day curing at room temperature. The anti-corrosion properties of the Cardanol-based coating containing the two-component microcapsules were tested using electrochemical impedance spectroscopy (EIS). It was found that, after 60-day immersion in 3.5 wt% NaCl solution, the low-frequency impedance modulus $|Z|_{0.01Hz}$ of the Cardanol-based coating containing GO-modified microcapsules was three orders of magnitude higher than that of the systems with capsules without GO. After scratching the coating containing 20 wt% GO-modified microcapsules and exposing it to an aqueous 3.5 wt% NaCl solution, the $|Z|_{0.01Hz}$ of the Cardanol-based coating returned over a period of 7 days to the original value.

1. Introduction

Epoxy-based coatings have been widely used for the corrosion protection of ships, buildings, drilling platforms, and chemical pipelines, due to their excellent water transport resistance, high cross-linking density, and outstanding mechanical properties and adhesion [1–4]. The currently used epoxy coating materials are mainly petroleum-based, which consume a large amount of non-renewable fossil resources and involve high pollution [5]. One of the effective ways to increase sustainability is to replace the use of petroleum-based feedstock with bio-based polymer feedstock such as Cardanol, vegetable oils, lignin, and cellulose [6–9].

Until now, different kinds of bio-based components including epoxy resins, diluents, and curing agents have been synthesized and widely used in various applications of epoxy coatings e.g. anti-corrosive coatings, composites, and adhesives [10,11]. The bio-based raw materials such as Cardanol and vegetable oils contain unsaturated double bonds and long alkane chains [12]. The application of these bio-based components will reduce the use of petroleum-based feedstock but may increase or decrease relevant properties of the coating [13,14]. For example, Zhang et al. reported that the use of epoxidized Cardanol components can significantly reduce the viscosity of the epoxy resin (E51), as well as improve the toughness of the coating [15]. Nameer et al. reported the preparation of epoxy coatings with high mechanical properties using vegetable oil-based reactive diluents [16]. However, compared to conventional epoxy coatings, bio-based components may lead to a poor compactness and high density of intrinsic defects leading to faster water migration, due to the low purity of bio-based materials

* Corresponding authors.
E-mail address: l.chu@njtech.edu.cn (L. Chu).

https://doi.org/10.1016/j.porgcoat.2023.107777
Received 4 May 2023; Received in revised form 20 June 2023; Accepted 24 June 2023
Available online 27 June 2023

[17,18]. The poor compactness and high intrinsic defect density will make them easier to form microscale cracks or delamination defects leading to loss of corrosion protection when exposed to practical conditions [19,20]. This will greatly reduce the performance of the coating and the effective lifetime from an anti-corrosion perspective.

Various strategies have been proposed and investigated to prolong the lifetime of epoxy coatings including the addition of functional fillers, polymer modification, self-healing capsules, etc. [21–23]. Recently, increasing attention has been paid to self-healing coatings due to their environmental stimuli-responsiveness and highly targeted intelligent healing [24,25]. Among them, extrinsic self-healing coatings in which the healing is achieved by the addition of microcapsules, which contain liquid restoration agents to fill and block the defects when a crack intersects them, are becoming increasingly popular due to their universality, low cost, high production rate, and high healing efficiency [26,27]. Their intrinsic drawback remains that local healing can only happen once as the healing agents are consumed and immobilised upon reaction. More healing strategies for coatings (including both extrinsic and intrinsic healing) can be found in a critical review paper [28].

Much research has been carried out on the design and preparation of microcapsules [29,30]. In his pioneering paper, White et al. [31] reported a self-healing system for an aerospace grade epoxy matrix using microencapsulated liquid dicyclopentadiene as well as a solid catalyst. Upon macroscopic cracking of the matrix, the microcapsule embedded in the sample broke, releasing the healing agent into the crack as a result of wetting. The subsequent contact with the catalyst causes polymerization over time and restoration of mechanical properties. In the fully healed condition, a 75 % toughness recovery was obtained. Rather than using a single capsule concept, the crosslinking reaction may enforce a dual capsule approach in which one set of capsules contains the resin and the other set the curing agent [32]. While the concept has the major drawback that adequate mixing of the two components cannot be ensured, such an approach offers more chemical freedom and was found to lead to interesting healing efficiencies. Thakur et al. [21] synthesized two-component microcapsules of epoxy resin and amine curing agent through in-situ polymerization and achieved a high healing efficiency of 82 % in the epoxy coating. In addition, the chemical resistance, tensile strength, and adhesion strength of the coating containing two-component microcapsules were also improved.

Until now, the studies of self-healing anti-corrosion coatings mainly focused on petroleum-based coating systems with naturally high corrosion resistance, while the reports on bio-based coatings with a naturally relatively low corrosion resistance are few [33]. One of the possible drawbacks of adding microcapsules to either petroleum or bio-based coatings is that they might reduce the electrolyte barrier properties of the coating, which is key for passive anti-corrosion coatings [34]. For instance, Arukalam found that the addition of microcapsules resulted in a 10^4 reduction in the impedance value of the epoxy coating, due to the formation of unwanted holes and transport channels in the composite coating [35]. Wang found that an epoxy coating containing microcapsules had a higher water uptake than pure epoxy coating during the immersion period, resulting in a ten-fold reduction of the impedance modulus at 0.01 Hz [36]. Thus, in addition to a proper capsule dimension and shape [37] (controlling the amount of healing agent released per fracture event), a proper volume fraction (controlling the amount of healing agent available to fill the crack [38,39]), the capsule wall providing a perfect protection of the capsule content against water and other external effects such as shear forces during coating deposition, and a good dispersion within the coating, the design of microcapsules for bio-based anti-corrosion coatings should consider the following aspects: 1. A high crosslinking capability between the healing agent and the bio-based coating matrix [40]; 2. A high interfacial bond strength between the unbroken microcapsules and bio-based coating [41]; and, 3. A minimal decrease in the barrier properties and mechanical properties of the coating due to the presence of microcapsules [42,43].

Graphene oxide (GO), due to its high functionality and high barrier properties, has attracted increasing attention as a useful ingredient in self-healing anticorrosion coatings [15,44]. Ma et al. [45] reported that due to the coverage of the capsule shell wall by GO, the microcapsule surface formed better bonds with the coating, and the diffusion rate of corrosion agents was reduced due to the dense structure of GO. Li et al. [46] fabricated microcapsules using GO as the shell material by self-assembly of GO at the oil-water interface with the assistance of benzotriazole (BTA). The GO capsules reached a high epoxy monomer loading capacity of 90.5 % and a healing efficiency of the composite coating of over 99.7 %. At present, as far as we know, all the designs of the self-healing microcapsules containing GO were designed for petroleum-based epoxy coatings. The design of GO-modified microcapsules for bio-based coatings addressing all the above three aspects is rarely reported.

In this paper, the design of the self-healing microcapsules meeting the three design criteria mentioned above is presented. Two types of microcapsules containing either Cardanol-based resin or Cardanol-based curing agents were prepared using the solvent evaporation method. Nanometer size epoxidized GO (E-GO)/Cardanol-based epoxy resin and aminated GO (A-GO)/Cardanol-based curing agent were encapsulated in two different sets of capsules respectively, so as to improve the barrier properties of the curing part of the coating after scratches. Amine-modified GO (M-GO) was further grafted on the shell surface by electrostatic adsorption, so as to improve the barrier properties of the capsule and the bond strength between the capsule and the matrix. Our results are relevant for the design of microcapsules for bio-based self-healing coating and will contribute to prolonging the lifetime of all types of bio-based epoxy coatings.

2. Experimental sections

2.1. Materials

Cardanol-based epoxy resin (602A), Cardanol-based amine curing agent (718A) and Cardanol-based surfactant (NSF3007C) were obtained from Nasurfar Biomaterials Technology (Changshu) Co., Ltd. Petroleum-based epoxy resin (E51) was purchased from Shenzhen Jitian Chemical Co., Ltd. Ethanol, with a purity higher than 99.7 %, was purchased from Wuxi Yasheng Chemical Co., Ltd. Polymethylmethacrylate (PMMA, mw ~ 130,000) was purchased from Tianjin Heowns biochemical technology co., ltd. Dichloromethane (DCM, AR, 99.5 %, containing 50–150 ppm isoprene stabilizer), N, N′-Dicyclohexylcarbodiimide (DCC, ≥99 %), *N*, *N*-Dimethylformamide (DMF, 99.5 %),) and 4-Dimethylaminopyridine (DMAP, 99 %) were purchased from Shanghai Aladdin Biochemical Technology Co., Ltd. Maleic acid diamine (MAD, 99 %) was purchased from Shanghai Macklin Biochemical Co., Ltd. Natural flake graphite (325 and 8000 mesh) was obtained from Shanghai Aladdin Biochemical Technology Co., Ltd.

2.2. Synthesis of modified graphene oxide

Graphene oxide (GO) was prepared from graphite flake powders through a modified Hummer's method [47]. GO grafted with MAD (M-GO) was synthesized according to the experimental method of Zhang et al. [44]. Fig. 1 shows the schematic diagram of the synthesis process of the modified GO (M-GO, E-GO, and A-GO).

For the preparation of M-GO, 2.5 g MAD was dissolved in 50 mL DI water, and magnetically stirred for 10 min to obtain a solution. The solution was slowly added into 100 mL GO (1 g/L) placed in a three-necked flask and refluxed at 80 °C for at least 8 h. The product was centrifuged for 10 min at 6000 rpm and washed with DI water 5 times and finally prepared into M-GO aqueous solution (1 g/L) under sonication for 10 min.

The synthesis of GO grafted with epoxidized Cardanol (602A) (E-GO) was under the experimental conditions of Zhang et al. [15]. GO ethanol

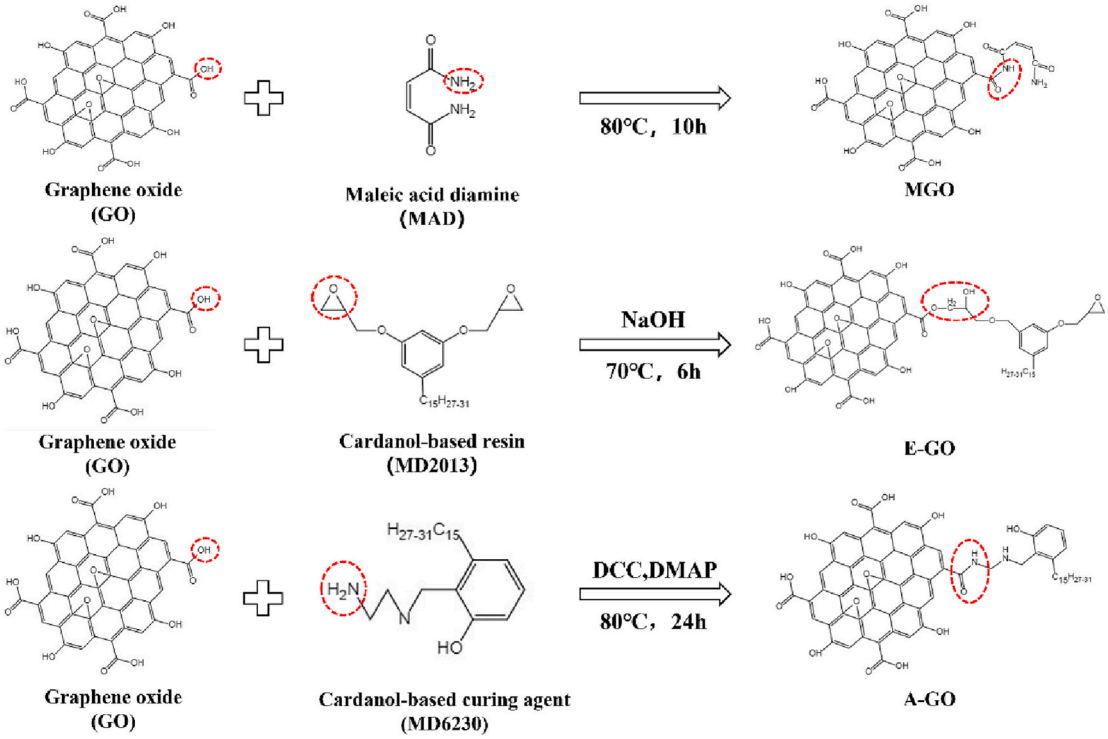

Fig. 1. Schematic diagram of the preparation process of M-GO, E-GO, and A-GO.

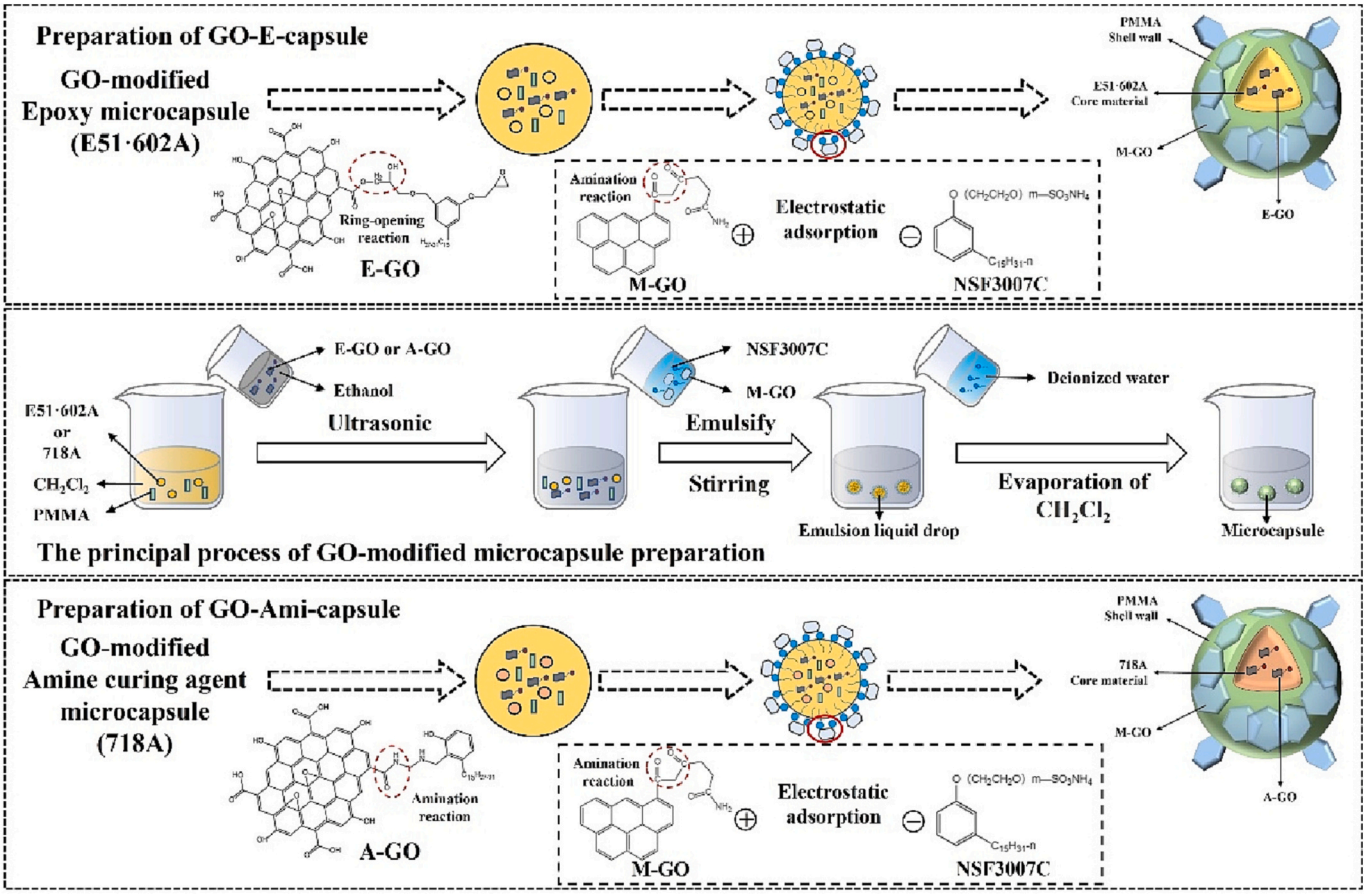

Fig. 2. Schematic diagram of the preparation of the GO-modified epoxy microcapsule (GO-E-capsule) and GO-modified amine curing agent microcapsule (GO-Ami-capsule).

solution (1 g/L) was sonicated for 30 min, followed by the dissolving of 602A using magnetic stirring at 600 r/min for 1 h. Then, the GO ethanol solution was transferred into a three-necked flask with magnetic stirring in a water bath at 70 °C for 6 h, NaOH aqueous solution was added drop by drop as the catalyst. After the reaction, the 602A and the catalyst were centrifugally washed with ethanol for 5 times until the unreacted 602A and catalyst were washed away. Afterward, 1 g/L E-GO ethanol suspension solution was prepared under sonication for 10 min.

GO grafted with aminated Cardanol (718A) (A-GO) was synthesized based on the work of Liu et al. [48]. First, GO was exfoliated by ultrasonication in a round-bottom flask filled with DMF with a concentration of about 1 g/L. Then, 718A, DCC (N, N′-dicyclohexylcarbodiimide), and DMAP (4-dimethylaminopyridine) (with the ratio of GO, 718A, DCC, and DMAP of 50 mg:1.5 mmol:1.5 mmol:1.5 mmol) were mixed in a flask and stirred at 80 °C for 24 h. The obtained solution was washed with ethanol for 5– 6 times and then diluted into 1 g/L solution under sonication for 10 min.

2.3. Synthesis of microcapsules containing E51/Cardanol-based epoxy resin and Cardanol-based curing agent

Fig. 2 shows the schematic diagram of the synthesis process and structure of the GO-modified bio-based microcapsules. First, 25 mL E-GO/ethanol suspension (1 g/L) was added to 30 mL of DCM. Then, the mixture was sonicated for 15 min to reach a good dispersion. 1 g PMMA and 1 g E51/ 602A (mass ratio of 7:3) were added to a 30 mL DCM solution under magnetic stirring. The mixture obtained was then mixed with 80 mL 5 wt% surfactant aqueous solution (NSF3007C) together with 25 mL M-GO aqueous solution (1 g/L), followed by being stirred at 4000 rpm for 10 min to obtain oil in water emulsion. 120 mL 5 wt% NSF3007C surfactant aqueous solution was added to the emulsion under mechanical agitation at 40 °C. After stirring for 4 h, the DCM was gradually allowed to evaporate and the GO-modified epoxy microcapsule (GO-E-capsule) suspension was obtained. The suspension obtained was centrifuged, and washed for five times. Before further applications, the microcapsules were dried at room temperature in vacuum for 24 h to remove any residual solvents (the GO content in the core material was about 2.5 wt%).

The Cardanol-based curing agent, 718A, was also encapsulated to prepare the GO-modified amine curing agent microcapsule (GO-Ami-capsule), using the same method as GO-E-capsule. In comparison, both microcapsules named E-capsule and Ami-capsule were prepared using Cardanol-based surfactant (NSF3007C) as the emulsifier without GO, respectively.

2.4. Preparation of self-healing coating

A warm-rolled construction Q235 steel plate was used as the metallic substrate. Before the coating application, the substrate was polished with 400 mesh sandpaper to remove the grease and oxide layer on the surface, washed with ethanol, and dried with hot air to remove any surface dust. 2 g GO-E-capsule, 2 g GO-Ami-capsule, and 3 g 602A Cardanol-based epoxy resin were mixed followed by stirring for 10 min at 500 rpm. Then 7 g E51 epoxy resin was added to the mixture. The mixture was stirred for 5 min at 500 rpm. Afterwards, 8.8 g 718A Cardanol-based amine curing agent was added to the mixture. The mixture was stirred for 5 min at 500 rpm and then vacuum dried for 10 min. A wet film with a thickness of 100 μm was applied by coating the mixture on the pretreated carbon steel plate using a four-sided scraper. The sample was dried at room temperature for 24 h to obtain a dry film coating with a thickness of 100 ± 5 μm. Herein, the coatings without and with different microcapsules were labeled as neat-coating, cap-coating, and GOcap-coating, respectively.

The volume fraction of the microcapsules used in this paper was about 20 %. The selected volume fraction of capsules was determined on the basis of the particle size of the microcapsules. For microcapsules with a particle size <50 μm, high healing efficiencies can only be achieved with a high volume fraction (~20 %) [49].

2.5. Characterization

2.5.1. Chemical structure and morphology analysis of modified GO

Fourier transform infrared spectroscopy (FT-IR), Raman spectroscopy, and X-ray photoelectron spectroscopy (XPS) were used to characterize the chemical structure of GO, M-GO, E-GO, and A-GO, respectively. A RQUINOX55 FT-IR Spectrometer, with 32 scans from 4000 to 400 cm^{-1}, was used at the resolution of 2 cm^{-1}. Horiba Labram HR800 Raman spectrometer with a green excitation laser (514 nm) was used for all the Raman characterizations. A PHI 5000 Versa Probe III X-ray photoelectron spectrometer (ULVAC-PHI, Japan) was used for all the XPS studies. Atomic force microscope (AFM, icon, Bruker) was used to characterize the microstructure and morphology of M-GO, E-GO, and A-GO with a Nanoscope IV controller. The water contact angle of GO, M-GO, E-GO and A-GO were measured using the SDC-350 contact angle meter (Sindin, China).

2.5.2. Microcapsule morphology characterization

The surface morphologies of the microcapsules were imaged and analyzed using a Hitachi S-4800 scanning electron microscope (SEM). The size distribution of microcapsules was measured using a laser particle size analyzer (Symantec Helos BF, range: 0.1 to 875 μm).

2.5.3. Thermal stability of the microcapsules

The thermal stability and loading capacity of produced modified microcapsules were characterized by a thermo gravimetric analyzer (TGA, NETZSCH STA 409PC). The samples were heated from 25 to 500 °C at a heating rate of 10 °C/min under an N_2 atmosphere.

2.5.4. Characterization of the anticorrosion properties of the coatings

To evaluate the anticorrosion properties of the prepared self-healing Cardanol-based coatings, electrochemical measurements were conducted on the coated steel panels using an electrochemical workstation (CHI-660E, Shanghai Chenhua Instrument Co., Ltd). The samples were clamped between a glass tube and an O-ring seal (a radius of 4 cm). The tube was partly filled with the test electrolyte (3.5 wt% NaCl solution) and sealed with a rubber stopper. A reference saturated calomel electrode (SCE) and a platinum counter electrode were used. The test process was carried out at room temperature, and the frequency of the AC impedance test ranged from 10^5 to 10^{-2} Hz with an amplitude of 20 mV. The samples were tested after 0, 1, 7, 15, 30, and 60 days of immersion. To further evaluate the anti-corrosion performance at damaged sites, scratches (3 cm length, 20 μm wide) were made manually on the surface of coatings using a sharp blade. Scratches were made down to the metallic substrate. Per coating composition, two sets of scratch samples were prepared. One of the scratched coatings was immersed in 3.5 wt% NaCl solution for up to 7 days. The other scratched coating was first cured at RT for 24 h prior to immersion in 3.5 wt% NaCl solution for up to 7 days. The EIS measurements were performed on both samples every day. Finally, the morphology of the cross-section of the coating after fracture was determined using SEM.

2.5.5. Characterization of the mechanical healing of the free-standing material in air

In order to evaluate the self-healing properties of the prepared epoxy materials, fracture tests were carried out on tapered double cantilever beam (TDCB) specimens having a thickness of 1 mm according to the procedure proposed by Soo Hyoun Cho et al. [50]. The T-shape sample was cured at room temperature for 24 h. Then, a pre-crack was created with a blade (Fig. S1). All fractured specimens were tested at a wedge displacement rate of 10 mm/min in a Universal material testing machine (KJ-1065). Upon reaching the peak load the sample was unloaded, which caused the newly formed crack surfaces to regain contact. The

sample was stored horizontally and healed at this condition at room temperature for 24 h to reach a fully cured state. Afterward, the strength of the healed specimen was tested and marked as S_{healed}. The healing efficiency is defined as the ratio of the maximum tensile strength of the healed sample and that of the original sample: $\eta = S_{healed}/S_{original} \times 100\%$.

3. Result and discussion

3.1. Characterizations of the microcapsules modified by GO

3.1.1. Chemical composition of modified GO

To demonstrate the successful modification of the GO materials, FT-IR was used to characterize the functional groups of GO, M-GO (GO modified with maleic acid diamine), E-GO (GO grafted with epoxidized Cardanol), and A-GO (GO grafted with aminated Cardanol). Fig. 3a shows the FT-IR spectra of M-GO, MAD and GO. The absorption peaks at 1730 and 3433 cm^{-1} represent the C═O group and O—H group vibrations of GO, respectively. Its height is reduced after the amine modification, which is consistent with the fact that the amine groups react with carboxyl groups to form an amide group. A new C—N bond stretching peak at 1464 cm^{-1} was observed in M-GO. The major characteristic peak of MAD at 1600 cm^{-1} (N—H bending vibration) appeared in M-GO. Thus, it can be concluded that M-GO has been successfully synthesized.

The FT-IR spectra of GO, E-GO, and Cardanol-based epoxy resin 602A are shown in Fig. 3b. The characteristic peaks of GO are located at 3424, 1728, and 1059 cm^{-1}, which correspond to O—H stretching mode of the C-OH, C═O stretching mode of the -COOH, and C-O-C vibration mode, respectively. After the 602A modification of GO, two new peaks at 2925 and 2853 cm^{-1} corresponding to the C—C and C—H bonds are observed. Meanwhile, a new absorption peak appeared at 1113 cm^{-1}, as a result of the reaction between the carboxyl group of GO and the epoxy ring of 602A. These results indicate that 602A was chemically bonded onto the GO surface.

The FT-IR spectrum of A-GO is shown in Fig. 3c to confirm the successful grafting of GO by 718A. After modification with 718A, the -COOH peak at 1728 cm^{-1} disappears and new peaks corresponding to C—C, C—H, and substituted benzene vibration at 2925, 2853, 772, and 697 cm^{-1}, suggesting that 718A has been successfully grafted onto GO surface.

The modified GO flakes of different sizes have been used to encapsulate the GO in the microcapsules and to coat them on the outside surface of the microcapsules. The morphologies of the prepared M-GO, E-GO, and A-GO were characterized using AFM. As shown in Fig. 3d, M-GO was recognizable as flakes with an average size of 5 μm. The size of E-GO and A-GO flakes were 450 and 415 nm, respectively. It is noted that to ensure a good barrier property after healing, the size of GO needs to be maximized. However, increasing the GO size will significantly affect the formation of a stable oil-water mixture, which will lead to the failure of the microencapsulation. Thus, the size of the GO flakes had been optimized by maximizing the size while ensuring a sufficient encapsulation rate.

As shown in Fig. 4b, the presence of C is shown by 1 s peak at 282–287 eV, that of N causes the 1 s peak at 397–402 eV, and that of O by the 1 s peak at 529–533 eV in the XPS spectra of GO, M-GO, E-GO, and A-GO. The C 1 s spectra of GO (Fig. 4c) were deconvoluted into three peaks at 284.8 eV, 286.9 eV, and 287.7 eV, which correspond to C—C, C—O, and C═O, respectively. In the spectrum of E-GO, the intensity of the characteristic peak of C—C (284.8 eV) increased significantly. This is due to the grafting of 602A on the surface of GO, which contains a large number of C—C bonds.

In Fig. 4d, the N 1 s XPS spectra of M-GO are deconvoluted into three fitting curves with peaks at 397.6 eV and 399.6 eV, attributed to C-NH_2 and C-N-C groups. The C-N-C groups were attributed to the covalent bonding between GO and MAD, while C-NH_2 originated from the MAD molecules. As shown in Fig. 4f, the N 1_S XPS spectrum of A-GO presents two different chemical peaks: C—N (397.1 eV) and C-NH_2 (399 eV). These phenomena indicate that 718A has been successfully grafted onto the surface of GO via amidation reaction, which was consistent with the FTIR results. The dispersibility of GO with different modifications in ethanol and water is shown in Fig. S2. The contact angles of GO, M-GO, E-GO, and A-GO are presented in Fig. S2. GO and M-GO in deionized

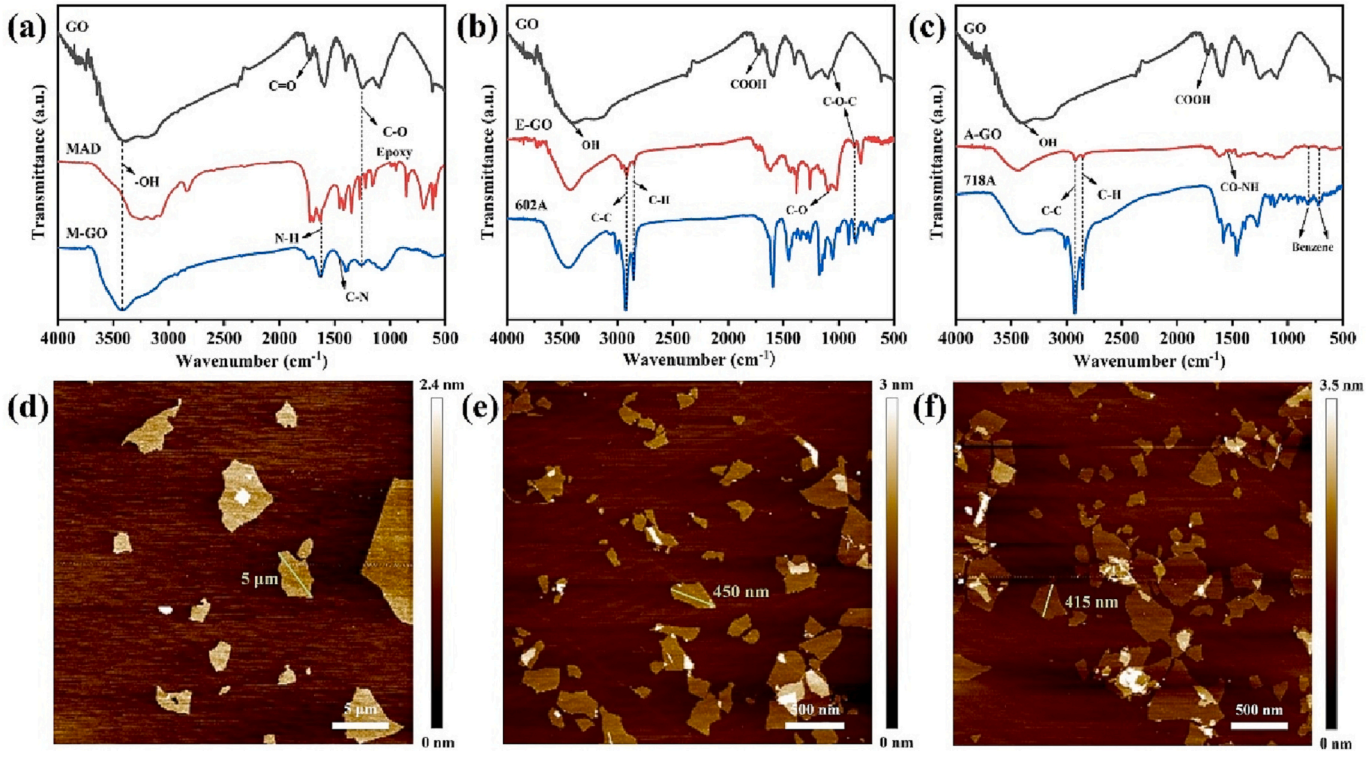

Fig. 3. FTIR spectra of (a) M-GO, GO; (b) E-GO, GO, and 602A; (c) A-GO, GO, and 718A; AFM morphologies of (d) M-GO, (e) E-GO and (f) A-GO.

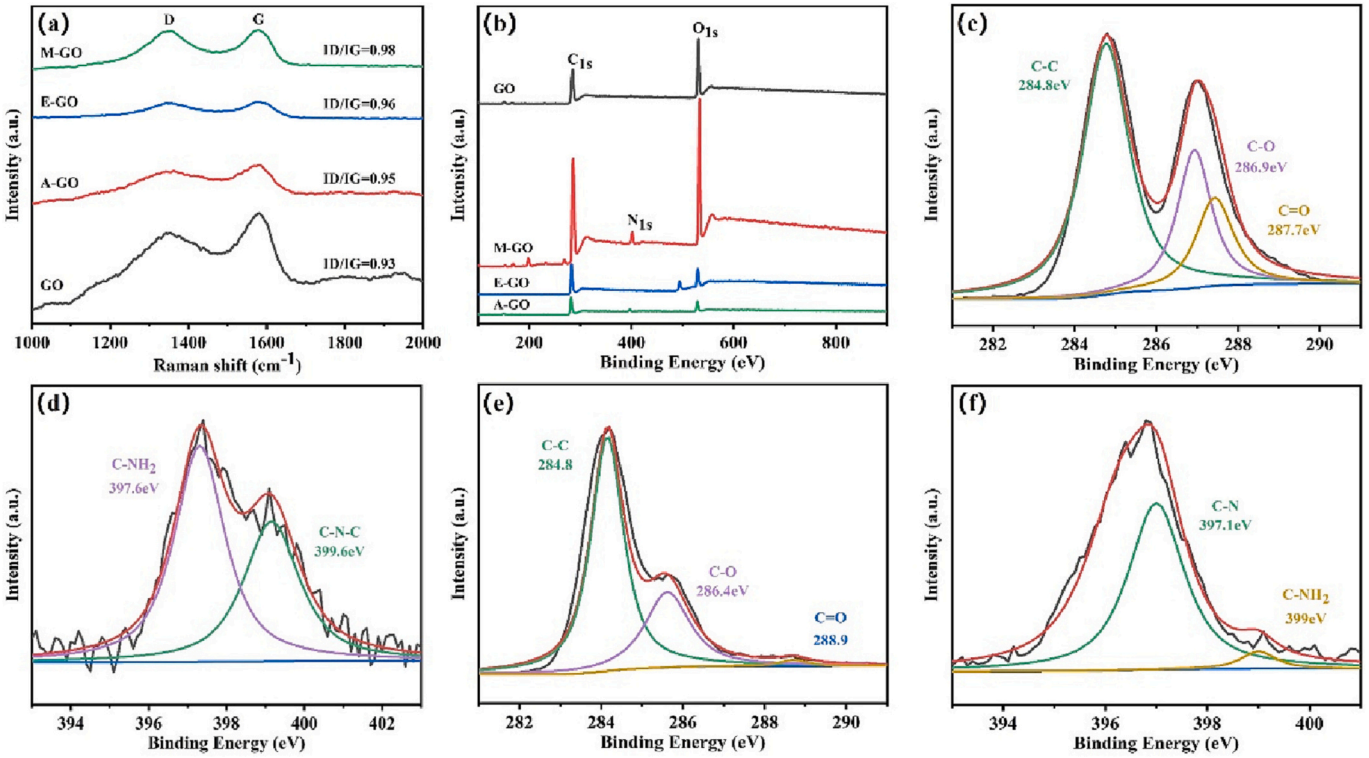

Fig. 4. (a) Raman spectra of M-GO, E-GO, A-GO, and GO; (b) XPS spectra of GO, M-GO, E-GO, and A-GO; (c) C 1 s XPS spectra of GO; (d) N 1 s XPS spectra of M-GO; (e) C 1 s XPS spectra of E-GO; (f) C 1 s XPS spectra of A-GO.

water, as well as E-GO and M-GO in ethanol all show good dispersibility. As shown in Fig. S2a, the water contact angle of the flat GO surface is 19°. After modification, the contact angle of M-GO remains at 17° as shown in Fig. S2b. This confirms that M-GO grafted with diamine maleate is still hydrophilic. As shown in Fig. S2(c, d), after modification, the water contact angles of E-GO and A-GO are 65° and 71°, respectively. This further confirms the successful modification of 602A and 718A which both have a long and hydrophobic chain. All these results confirm the reaction mechanisms proposed in Fig. 1.

3.1.2. *Topological and thermal properties of the microcapsules*

As mentioned above, in principle the addition of microcapsules will significantly reduce the barrier property of the epoxy coating, due to the low barrier property of the microcapsule itself and the poor interfacial bonding between the PMMA shell and the Cardanol-based coating [51]. In this paper, the strategy to solve this key issue is to encapsulate modified GO nano-flakes in the core of the microcapsules and to cover modified GO flakes on the surface of the microcapsules. To demonstrate the successful coverage of the modified GO flakes, SEM has been used to characterize the surface morphology of the microcapsules as shown in Fig. 5a. In the SEM images, spherical microcapsules with uniform size distribution and without any aggregations are visible. The cross-section of the shell as shown in Fig. 5b demonstrates that the average shell thickness of microcapsules was 300 ± 5 nm. As shown in Fig. 5c and d, both microcapsules loaded with E51/602A and microcapsules loaded with 718A have smooth surfaces, and the shell is flawless without any cavity.

Fig. 5e and f show the SEM images of the microcapsules covered by M-GO. The surface of the microcapsules became rougher compared to the surface of microcapsules without GO. As shown in the optical image at the upper left corner of Fig. 5e, GO-E-capsule was in a gray powder state, which is different from the white powder in Fig. 5c. As shown in the image at the upper left corner of Fig. 5f, the powder of GO-Ami-capsule also shows a gray color, which is to be compared with the yellow microcapsules loaded with 718A. SEM images show that there are large pieces of M-GO flakes wrapped on the surface of the microcapsule. It can be inferred from Fig. 5 that the appropriate amount of modified GO material was added in the preparation process of the microcapsule, and the M-GO was successfully inserted and wrapped on the outer surface of the microcapsule by adjusting the hydrophilicity and electrostatic adsorption, and had no effect on the shapes and size distribution of the microcapsules. The morphology of microcapsules with different M-GO contents can be found in Figs. S3 and S4.

The particle size distribution of the GO-E-capsule and GO-Ami-capsule was tailored by the stirring speed [52]. As shown in Fig. 6a, the stirring speed of 4000 rpm was used and the average size of GO-E-capsule and GO-Ami-capsule was 4 μm and 4.5 μm with a narrow size distribution, respectively. The healing efficiency of the self-healing coating is strongly influenced by the amount of core material in the microcapsule. Thermogravimetric Analysis (TGA) has been applied to investigate the stability and the core content of the microcapsules using the method proposed by Boumezgane [34]. The mass loss curves of the three material grades are plotted in Fig. 6b and c as a function of temperature, and no significant weight loss of microcapsules was observed up to a temperature of 200 °C. As shown in Fig. 6b, the PMMA began to show some weight loss at 218 °C, and it decomposed completely at temperatures above 417 °C. The thermal weight loss of the GO-E-capsule could be separated into two stages. The first stage began at 219 °C, which was attributed to the evaporation of the PMMA. When the temperature increased to about 417 °C, PMMA was almost completely degraded. The second mass loss stage was at the temperature range of 417 °C (68 %) - 486 °C (10 %), which corresponded to the degradation of the E51/602A and E-GO encapsulated in the PMMA shell. The loading capacity of E51/602A was calculated to be 58 %. As shown in Fig. 6c, the neat PMMA utilized for this work completely decomposed at nearly 437 °C, with a final residual weight of 4.5 %. Considering the TGA curve of microcapsules loaded with 718A and A-GO, a much higher reside (54 %) was observed at 437 °C, followed by a 48 % decrease for temperatures up to 493 °C. Consequently, the core loading of GO-Ami-capsule was estimated at about 48 % from these results. The results show that

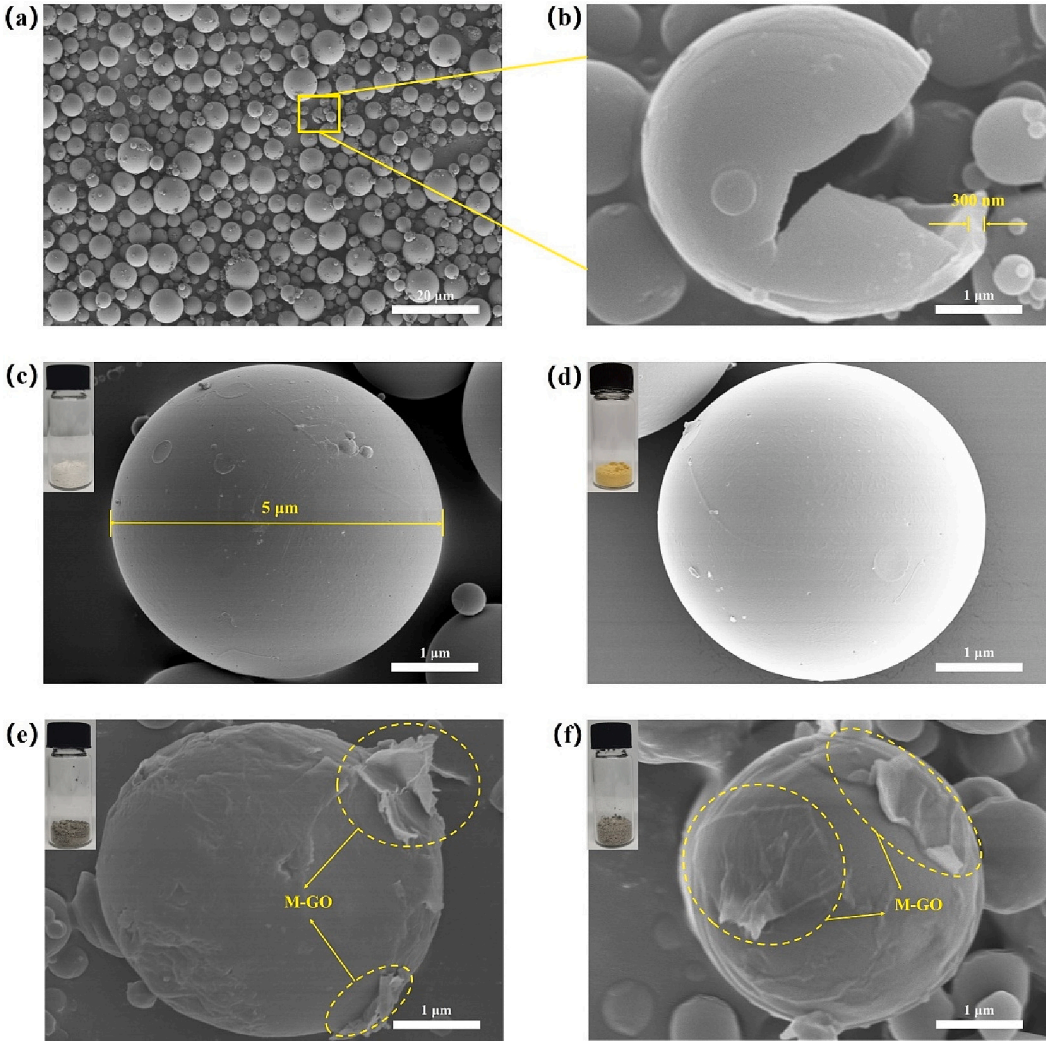

Fig. 5. SEM images of different microcapsules (a) overview of epoxy resin microcapsules, (b) individually broken microcapsule of (a), (c) microcapsule loaded with Cardanol-based resin (E51/602A), (d) microcapsule loaded with the Cardanol-based curing agent (718A), (e) GO-E-capsule and (f) GO-Ami-capsule.

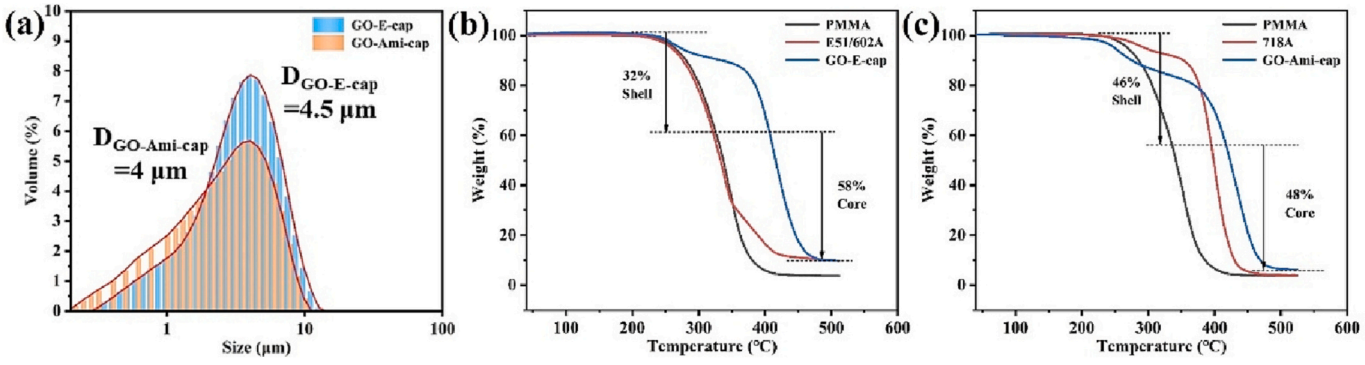

Fig. 6. Particle size distribution at different speeds of (a) GO-E-capsule and GO-Ami-capsule; TGA weight loss curve of (b) PMMA, E51/602A, and GO-E-capsule; (c) PMMA, 718A, and GO-Ami-capsule. (The capsules were prepared at a stirring rate of 4000 rpm).

the microcapsules were successfully encapsulated the core materials. As shown in Fig. S6, FT-IR spectra proved that GO-E-capsule and GO-Ami-capsule were successfully encapsulated by PMMA with Cardanol-based healing agent and nano-sized GO, and the outer surface of the microcapsules contained M-GO.

3.2. The role of GO on the overall properties of the self-healing coatings

3.2.1. Enhancement of the anti-corrosion performance of the intact coating

The target mechanism to increase the anti-corrosion properties (barrier) of the intact coatings with GO-modified microcapsules is schematically illustrated in Fig. 8e. Herein, the main purpose of introducing GO materials onto the self-healing microcapsules is to solve the

issue that the addition of the conventional microcapsules will significantly decrease the barrier properties of the epoxy coating. Due to the non-crosslinked nature of the healing agent encapsulated in the microcapsules, the barrier properties of the microcapsules themselves are much lower than the coating matrix. As a result, the diffusion coefficient of the corrosion ions is high in the microcapsules, as shown in Fig. 7d. Being a dense 2D material, the GO has a very high barrier property due to its unique hexagonal ring structure. The addition of GO covered on the surface of the microcapsules will block the corrosion medium from transmitting via the microcapsules, which will improve the barrier properties of the self-healing coatings. The barrier performance of the coatings was evaluated using electrochemical impedance spectroscopy (EIS) during immersion in 3.5 wt% NaCl aqueous solution [53]. The coatings without and with microcapsules prepared using different additives including NSF3007C, and NSF3007C + GO are labeled as 'neat-coating', 'cap-coating', and 'GOcap-coating', respectively. The dry film thickness of the neat-coating, cap-coating, and GOcap-coating are 101, 100, and 100 μm, respectively. The Nyquist and Bode (|Z| and phase angle) plots of intact neat-coating, cap-coating, and GOcap-coating are shown in Fig. 7. In a first-order approximation, in the Nyquist plot, the number of capacitive arcs determines the number of time constants and a large radius of the capacitive arc indicates better anti-corrosion performance. As shown in Fig. 7b1, after 1 day of immersion, the Nyquist diagram of the cap-coating shows two capacitive arcs. This indicates that the electrolyte has penetrated into the coating and reached the metal-coating interface. Contrary to this, Fig. 7a1 and c1 for the neat-coating and GOcap-coating respectively, only show one capacitive arc even after the 60 days of immersion. A similar observation can be made using the phase angle (Fig. 7a2, b2, and c2) and total impedance (Fig. 7a3, b3, and c3) evolution with the immersion time. The cap-coating sample shows a rapid drop of both phase angle and total impedance at mid-frequencies, a clear sign of loss of the barrier protection. On the other hand, both neat-coating and GOcap-coating show capacitive behavior (phase angle near 90, and total impedance linearly increasing with the frequency decrease). The above results also indicate that the addition of non-surface modified microcapsules (cap-coating) plays a negative role in the barrier performance of the coating, which is consistent with the previous reports [35].

In spite of the similarities, the neat-coating and the GOcap-coating also show slight variations in the impedance results. In general, the impedance modulus at f = 0.01 Hz ($|Z|_{0.01Hz}$) (Fig. 7a3, b3, and c3) reflects the coating's ability to suppress electrochemical charge transfer at the metal-coating surface and is an indicator of the level of corrosion protection. The greater the impedance modulus of the coatings is, the better the anticorrosion properties are. For the neat-coating, the initial $|Z|_{0.01Hz}$ value was 3.99×10^{10} Ω·cm^2 and dropped to 3.06×10^{10} Ω·cm^2 after 60 days of immersion, a sign that the electrolyte has not penetrated through the coating to the coating-substrate interface. When capsules

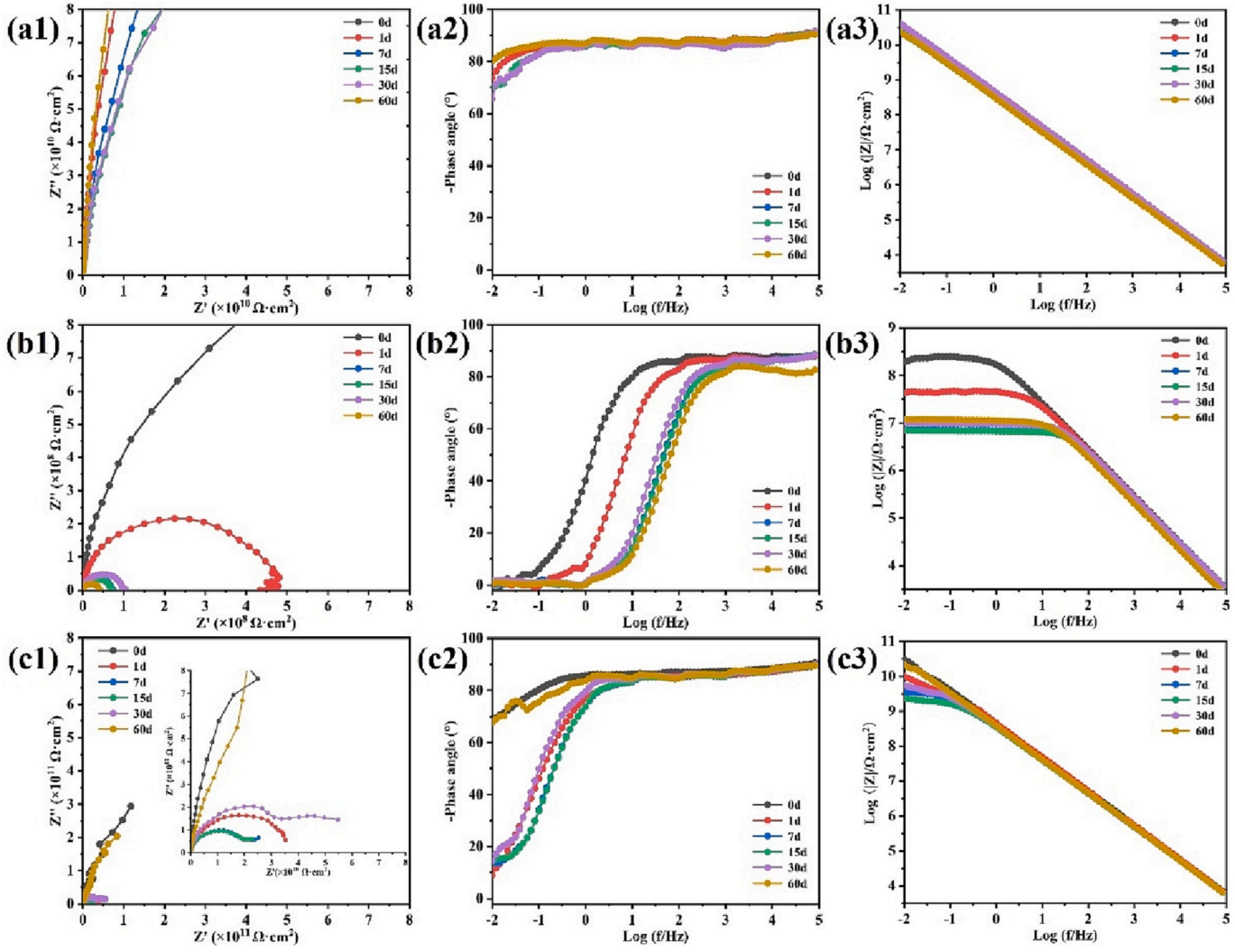

Fig. 7. Time evolution of the Nyquist (−Z'' vs. Z') and Bode (|Z| and phase angle) plots of (a1-a3) neat-coating, (b1-b3) cap-coating, and (c1-c3) GOcap-coating immersed in 3.5 wt% NaCl solution.

without surface GO modification are added (cap-coating), the initial $|Z|_{0.01Hz}$ starts relatively low (1.91×10^8 Ω·cm^2) and rapidly decreased one order of magnitude. This trend is in agreement with the relatively lower barrier protection offered by the coating with non-modified capsules attributed to the reduced compactness caused by the poor compatibility between the Cardanol-based coating and the PMMA shell of the capsules. This negative effect is inverted when the capsules are surface modified with GO. As shown in Fig. 7c3, the initial $|Z|_{0.01Hz}$ value of the GOcap-coating is comparable to the neat-coating (3.08×10^{10} Ω·cm^2) and remains as high as 2.14×10^9 Ω·cm^2 during the 60 days of immersion. Such a high and relatively stable impedance is related to good barrier properties ascribed to the fact that 2D GO materials with high-barrier properties can effectively enhance the density at the coating-capsule interface by cross-linking with the coating matrix. Thus, GO significantly slows down the diffusion rate of electrolyte at the microcapsule-epoxy resin interface. The equivalent circuit models are used to explain the electrochemical response of neat-coating, cap-coating and GOcap-coating during the immersion process in Fig. 8 a-c. The ZSimpwin software has been used to fit the data and the fitted electrochemical parameters are listed in Table S2.

3.2.2. *Enhancement of the load transfer between matrix and microcapsules*

The bond strength between the microcapsules and the coating matrix determines the load transfer, the time dependent rupture, and the release rate of the microcapsules, which are key for the healing efficiency. To investigate the effect of modified GO on the bond strength between microcapsules and Cardanol-based coatings, the morphology of the cross-section of the coating with different microcapsules was characterized using SEM. Fig. 9a shows the cross-section of the coating with non-GO-coated microcapsules. A large number of unbroken microcapsules are visible in the cross-section. A gap of about 0.5 μm between the Cardanol-based coating matrix and the microcapsule was observed. These results suggest that the microcapsule without GO has a poor bond strength to the coating matrix. The polymer matrix with GO-modified capsules behaves significantly different (Fig. 9b1, b2). As shown in Fig. 9b1, most of the microcapsules appear broken, as indicated by the broken hemispherical section. As marked in the yellow circle in Fig. 9b2, after the breakage of the microcapsule, the deformation of the polymer parts adhering to the microcapsule due to the stretching force is still visible. This indicates a strong bond strength between the microcapsule and the matrix. Moreover, as marked in the red circle in Fig. 9b2, part of the shell of another microcapsule was removed. This indicates that the bonding strength between the polymer matrix and the GO-modified microcapsules was strong enough to ensure the opening of the microcapsule when the crack of the coating was initiated. As shown in Fig. S5, there are many unbroken microcapsules in the cross-section of the coating without modified microcapsules, which is significantly different from the coatings with modified microcapsules. The above results indicate that the modified GO significantly enhanced the interface bonding between the microcapsule and the polymer coating matrix. This allows for a rapid capsule breakage due to load transfer once an external force is applied thereby ensuring excellent self-healing agents release from the GO-modified microcapsules.

3.2.3. *Healing efficiency of the mechanical strength in free-standing polymers*

The self-healing mechanism of the coatings with GO-modified microcapsules is schematically illustrated in Fig. 10 (a-c). In general, in extrinsic coatings, the healing efficiency is largely dependent on the breakage rate of the microcapsules in the vicinity of a crack, which in the case of comparable capsule shell strength, is in turn related to the capsule-matrix interface bonding strength. Fig. 10d shows the stress-strain curves of the original and healed samples with modified GO-microcapsules and with non-modified microcapsules. The tensile strength and elongation at a break of the original non-modified microcapsule sample are 0.274 MPa and 3 %. The strength of the healed sample is 0.139 MPa, which indicates a healing efficiency of about 50 %. When GO is added to the microcapsule surface (modified sample), the stress-strain curves of the original and healed samples, show an increase in initial and higher healing efficiency (80 %). The above results demonstrate nicely the improvement in healing efficiency due to the higher amount of capsules broken in the case of GO-modified microcapsules.

Fig. 10e shows the effect of the microcapsule content on the healing efficiency. As it can be seen, the healing efficiency for the 5 wt% was poor (23 %). By increasing the number of modified microcapsules, a higher healing efficiency could be obtained. The highest healing efficiency (80 %) was obtained when the microcapsule content was 20 wt% and dropped when more capsules were added. The mechanical healing efficiency of the coating containing normal (non-modified)

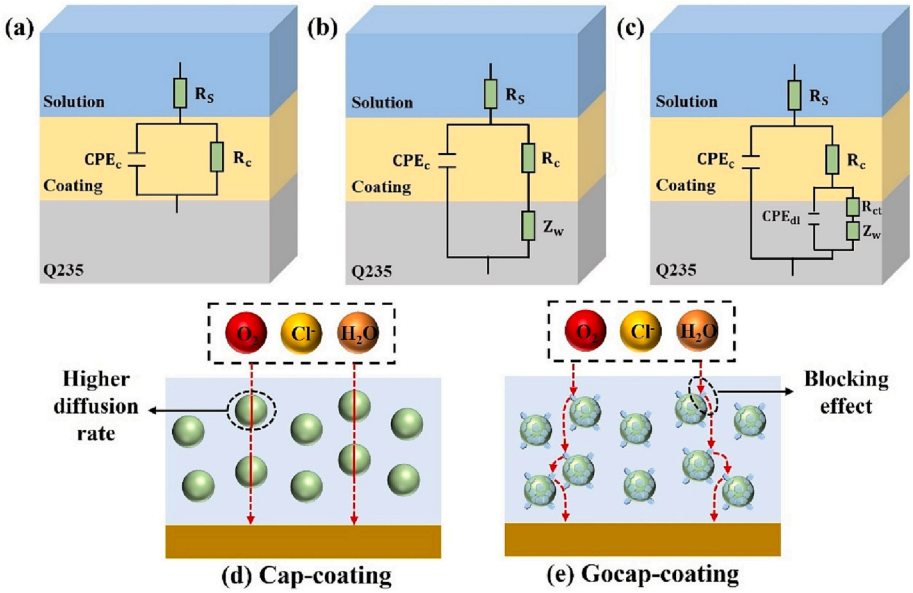

Fig. 8. Equivalent circuit models of (a) neat-coating, (b) cap-coating, and (c) GOcap-coating; schematic diagram of the diffusion path of corrosion medium in (d) cap-coating, and (e) GOcap-coating.

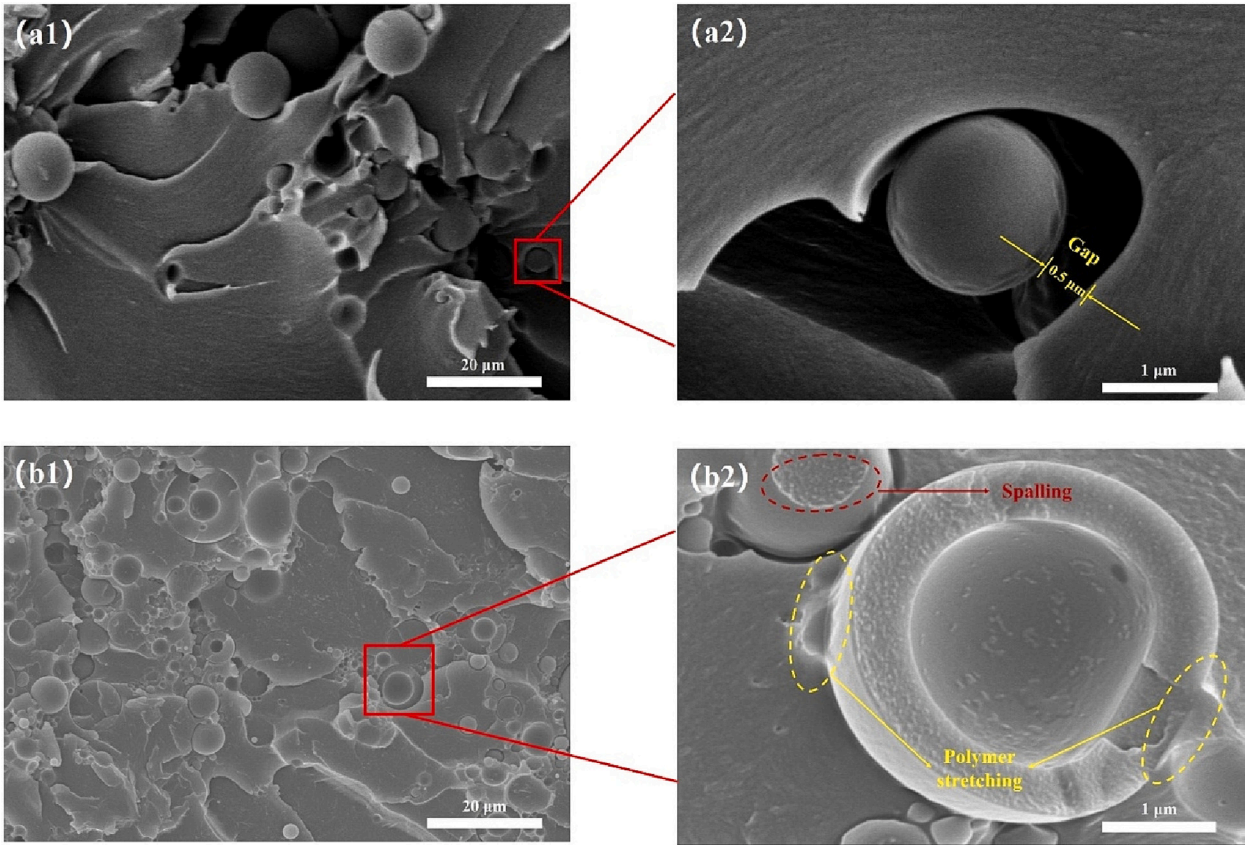

Fig. 9. Cross-section SEM images of (a1, a2) Cardanol-based coating containing E-capsule and Ami-capsule, (b1, b2) Cardanol-based coating containing GO-E-capsule and GO-Ami-capsule.

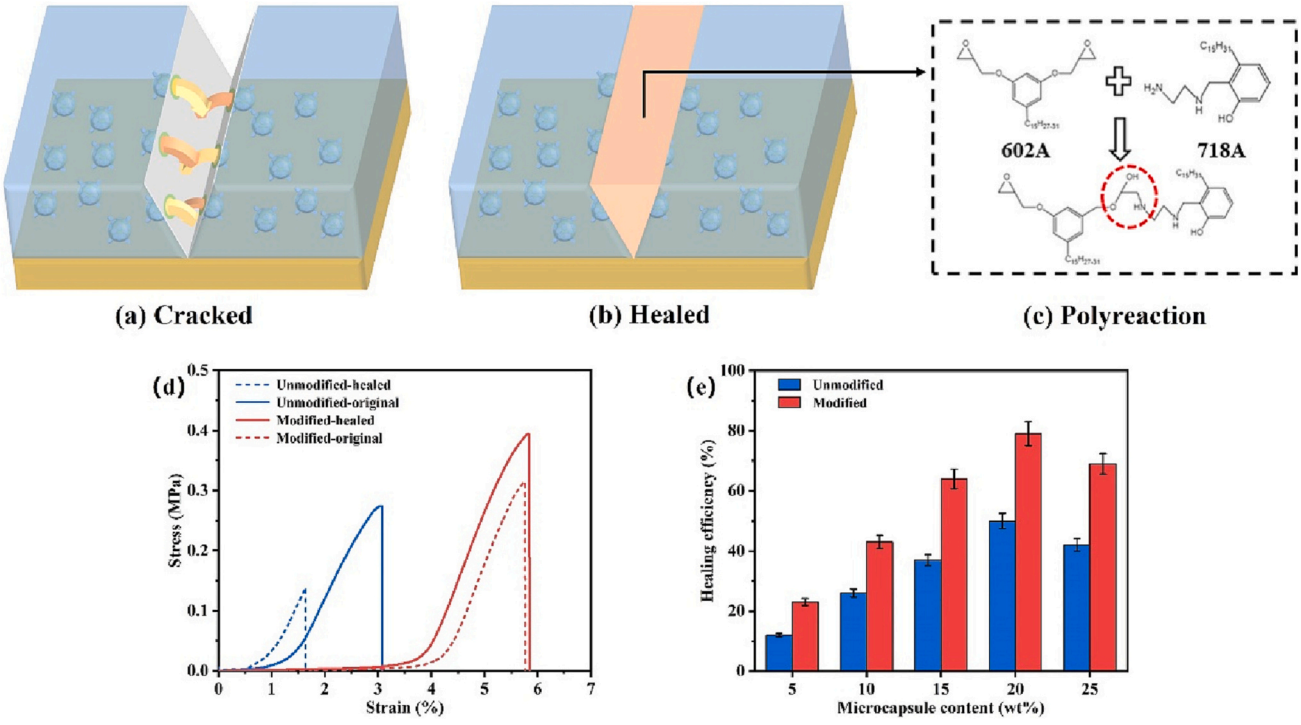

Fig. 10. (a-c) Schematic diagram of the self-healing mechanism of the composite coating with GO-modified microcapsules. (d) Stress–strain curves of self-healing TDCB fracture tests of the coatings with unmodified and modified microcapsules (20 wt%); (e) The healing efficiencies (%) of the coatings with 5, 10, 15, 20, and 25 wt% unmodified and modified microcapsules in autonomous TDCB test specimens healed at 25 °C for 24 h.

microcapsules is always lower than that of the coating embedded with GO-modified microcapsules.

3.2.4. Recovery of the barrier protection at damaged sites with GO-modified microcapsules

The proposed mechanism of enhancing the anti-corrosion properties (barrier) of the coatings at damaged sites when using GO-modified microcapsules is schematically illustrated in Fig. 14 (a-c). It is expected that the surface modification of the microcapsules by GO will enhance capsule rupture during scratching while the GO encapsulated in the microcapsules will locally increase the corrosion resistance at the damaged site upon release. As shown in Fig. 12, 'X' scratches were made on the surface of the neat-coating and self-healing coating with GO-modified and unmodified microcapsules, respectively. Then, the samples were immersed in 3.5 wt% NaCl solution for 7 days and monitored using EIS. According to Fig. 11a, the $|Z|_{0.01Hz}$ value of the scratched neat Cardanol-based coating shows a dramatic decrease of approximately 6 orders of magnitude (from $>10^{10}$ Ω·cm^2 to no $>10^4$ Ω·cm^2). The cap-coating (Fig. 11b) on the other hand, shows an initially lower $|Z|_{0.01Hz}$ of 4×10^7 Ω·cm^2 which drops to 1×10^4 Ω·cm^2 to later on gradually increase to 1.5×10^5 Ω·cm^2. The slight increase of $|Z|_{0.01Hz}$ value for the cap-coating can be ascribed to the self-healing of the scratch. The GOcap-coating (Fig. 11c), shows an initial $|Z|_{0.01Hz}$ value comparable to the neat–coating (3×10^{10} Ω·cm^2) followed by a sudden large drop of 7 orders of magnitude down to 8×10^3 Ω·cm^2 on the first immersion day. Nevertheless, the $|Z|_{0.01Hz}$ value of GOcap-coating increased again after 3 days of immersion to reach an impedance value as high as 1.23×10^9 Ω·cm^2 after 7 days of immersion. This result suggests that the healing agent in GO-modified microcapsules has a better release efficiency than that in the unmodified microcapsules. In addition, the impedance increase in time indicates proves that the healing process of the GO-loaded healing agent in the self-healing coating can still take place under seawater immersion conditions.

To compare the normal healing effect during exposure to air, after making 'X' scratches on the surface, the GOcap-coating was healed at room temperature for 24 h. As shown in Fig. 11d, the $|Z|_{0.01Hz}$ value of healed GOcap-coating always stayed at around 2.47×10^{10} Ω·cm^2 upon immersion in 3.5 wt% NaCl solution for seven days, similar to the behavior of the original coating. Fig. 12 shows the digital photos of different coating samples immersed in 3.5 wt% NaCl solution for 7 days. As shown in Fig. 11a2, after 7 days of immersion, the neat-coating has multiple locations of rust, the unmodified Cap-coating showed only one corrosion location, and the modified GOcap-coating has no corrosion. This shows that the modified GO inserted and wrapped on the surface of

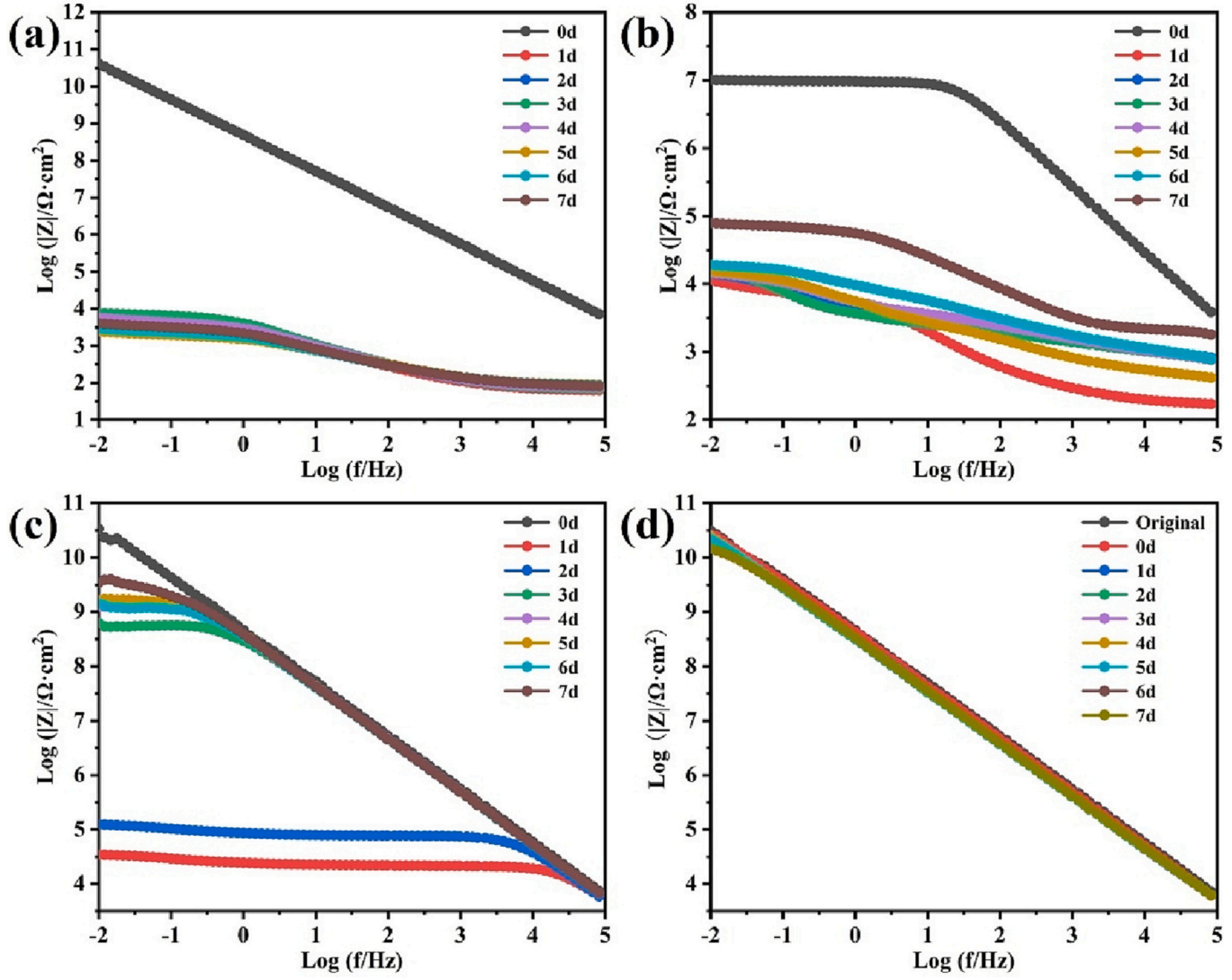

Fig. 11. Total impedance (|Z|) variation with the immersion time in 3.5 wt% NaCl solution of samples with a 'X' scratch with (i) no previous healing time: (a) neat-coating, (b) cap-coating, (c) GOcap-coating and (ii) with 24 h healing at room temperature: (d) GOcap-coating.

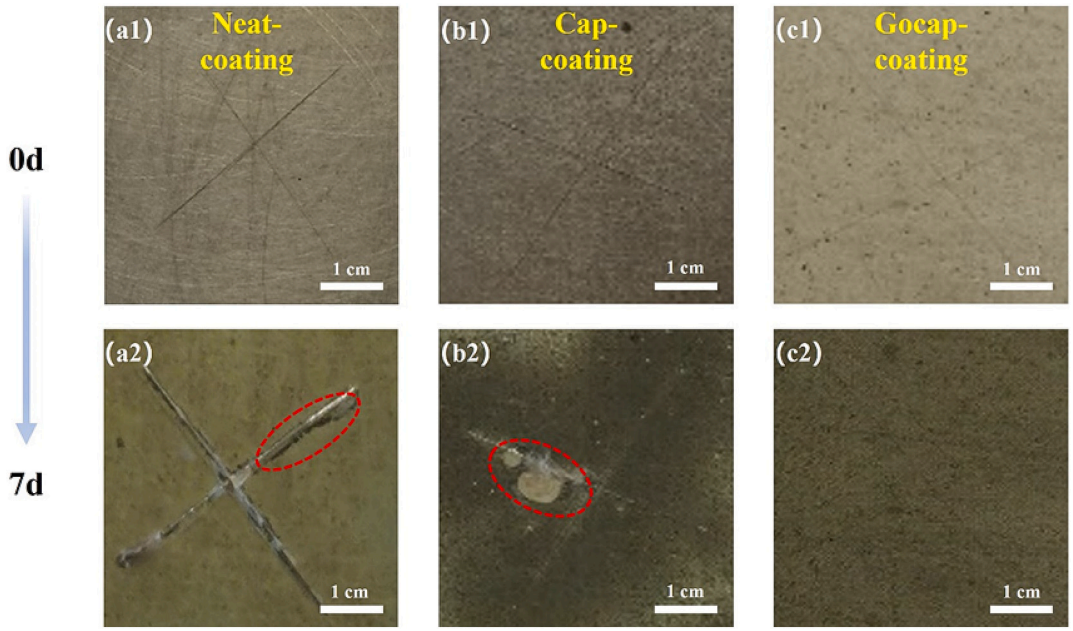

Fig. 12. Digital photos of (a1-a2) neat-coating, (b1-b2) cap-coating, and (c1-c2) GOcap-coating samples with 'X' scratches after immersion in 3.5 wt% NaCl solution for 7 days.

microcapsules in GOcap-coating can effectively improve the healing efficiency and corrosion resistance recovery at damaged sites.

Fig. 13 shows the microscope images and digital photos of GOcap-coating loaded with 20 wt% GO-modified microcapsules before and after healing at room temperature with an 'X' scratch on the surface. As shown in Fig. 13c, the width of the 'X' scratch on the coating surface is about 1.25 mm under the optical microscope. After 24 h of the healing process at room temperature, the 'X' scratch on the surface of the coating almost disappeared as shown in Fig. 13d. This showed that the modification of graphene and the increase of microencapsulation content have an excellent effect on the self-healing behavior.

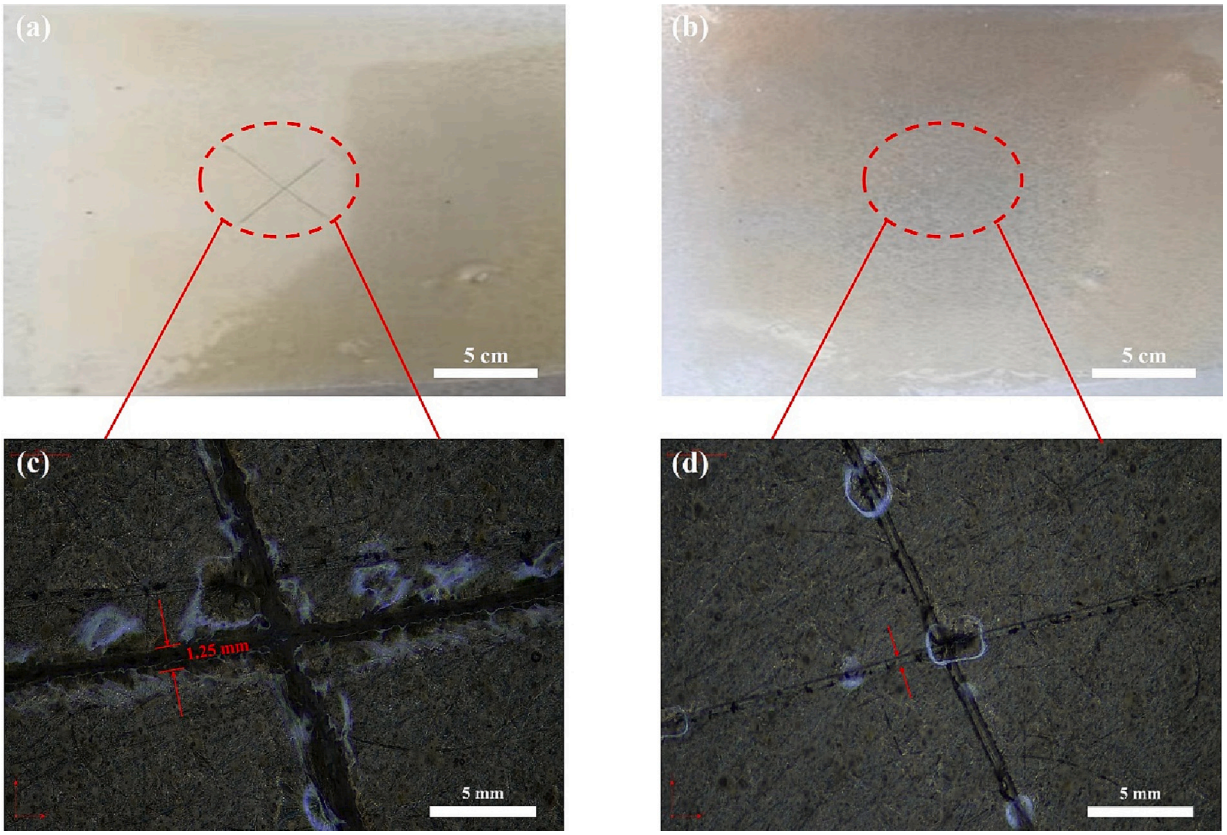

Fig. 13. (a, b) High-resolution optical images and (c, d) digital images of the GOcap- coating (20 wt%) before and after healing.

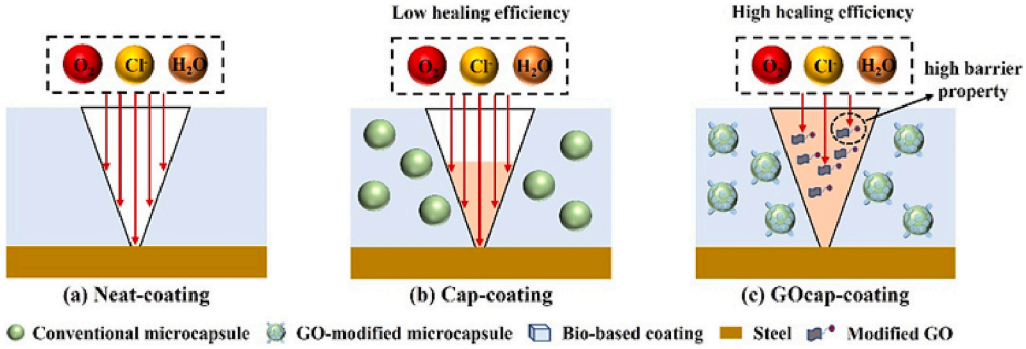

Fig. 14. Schematic diagram of the corrosion mechanism of the (a) neat coating, (b) cap-coating, and (c) GOcap-coating.

4. Conclusion

Cardanol-based coating with GO-modified microcapsules showing enhanced self-healing properties and outstanding anticorrosion properties both before and after the repair has been prepared. Microcapsules with modified GO both encapsulated in the core (as part of the healing agent) and coated on the shell were prepared. Modified GO was introduced around microcapsule shells to avoid the negative impact of microcapsules on the barrier properties of intact coatings. By using various chemical and morphological analyses, it was demonstrated that the introduction of modified-GO including epoxidized-GO and aminated-GO, can significantly enhance the bonding between the PMMA shell and the matrix. Thus, the microcapsules can be efficiently opened upon scratching or fracture. Moreover, the anticorrosion properties of the coating, both before and after healing, were greatly improved due to the presence of GO both in the core and the shell. In particular, compared to conventional microcapsules without GO, the low-frequency impedance modulus $|Z|_{0.01Hz}$ of the Cardanol-based coating embedded with GO-modified microcapsules increased three orders of magnitude after being immersed in 3.5 wt% NaCl solution for 60 days. The $|Z|_{0.01Hz}$ value of the healed Cardanol-based coating embedded with GO-modified microcapsules was 10^5 higher than the healed coating with no-GO microcapsules after being immersed in 3.5 wt% NaCl solution for 7 days. Moreover, healing with the GO-modified capsules took place during immersion in NaCl solutions as well as in the air, thereby demonstrating the high application versatility of this concept. This constitutes the highest performance of PMMA-based microcapsules in the literature. Our results reconfirm the excellent potential of GO materials in the field of self-healing microcapsules and the results in this work may give a guide to the design of multi-functional self-healing microcapsules.

CRediT authorship contribution statement

Wentao Wu: Writing – original draft, Data curation, Investigation, Conceptualization, Methodology. **Liangyong Chu:** Conceptualization, Investigation, Writing – review & editing, Supervision, Project administration. **Santiago J. Garcia:** Conceptualization, Investigation, Writing – review & editing. **Sybrand van der Zwaag:** Conceptualization, Investigation, Writing – review & editing. **Liming Shen:** Conceptualization, Investigation, Writing – review & editing. **Ningzhong Bao:** Conceptualization, Investigation, Writing – review & editing, Supervision, Project administration.

Declaration of competing interest

The authors declare that they have no known competing financial interests or personal relationships that could have appeared to influence the work reported in this paper.

Data availability

Data will be made available on request.

Acknowledgments

This research was supported by the National Key Research and Development Program of China (Grant No. 2020YFE0100100).

Appendix A. Supplementary data

Supplementary data to this article can be found online at https://doi.org/10.1016/j.porgcoat.2023.107777.

References

[1] Y. Zhou, G. Chen, S. Yan, C. Ni, L. Yu, X. Li, Epoxy composite coating with excellent anticorrosion and self-healing properties based on acrylate copolymers, Prog. Org. Coat. 172 (2022), 107098.
[2] X. Zhu, Q. Yan, L. Cheng, H. Wu, H. Zhao, L. Wang, Self-alignment of cationic graphene oxide nanosheets for anticorrosive reinforcement of epoxy coatings, Chem. Eng. J. 389 (2020), 124435.
[3] H. Chen, H. Fan, N. Su, R. Hong, X. Lu, Highly hydrophobic polyaniline nanoparticles for anti-corrosion epoxy coatings, Chem. Eng. J. 420 (2021), 130540.
[4] G. Contri, G.M.O. Barra, S.D.A.S. Ramoa, C. Merlini, L.G. Ecco, F.S. Souza, A. Spinelli, Epoxy coating based on montmorillonite-polypyrrole: electrical properties and prospective application on corrosion protection of steel, Prog. Org. Coat. 114 (2018) 201–207.
[5] C. Verma, L.O. Olasunkanmi, E.D. Akpan, M. Quraishi, O. Dagdag, M. El Gouri, E.-S.M. Sherif, E.E. Ebenso, Epoxy resins as anticorrosive polymeric materials: a review, React. Funct. Polym. 156 (2020), 104741.
[6] S. Danov, O. Kazantsev, A. Esipovich, A. Belousov, A. Rogozhin, E. Kanakov, Recent advances in the field of selective epoxidation of vegetable oils and their derivatives: a review and perspective, Catal. Sci. Technol. 7 (17) (2017) 3659–3675.
[7] R. Shen, M. Long, C. Lei, L. Dong, G. Yu, J. Tang, Anticorrosive waterborne polyurethane coatings derived from castor oil and renewable diols, Chem. Eng. J. 433 (2022), 134470.
[8] W. Wang, F. Wang, C. Zhang, J. Tang, X. Zeng, X. Wan, Versatile value-added application of hyperbranched lignin derivatives: water-resistance adhesive, UV protection coating, self-healing and skin-adhesive sensing, Chem. Eng. J. 404 (2021), 126358.
[9] B. Thomas, M.C. Raj, K.B. Athira, M.H. Rubiyah, J. Joy, A. Moores, G.L. Drisko, C. Sanchez, Nanocellulose, a versatile green platform: from biosources to materials and their applications, Chem. Rev. 118 (24) (2018) 11575.
[10] D.A. Bellido-Aguilar, S. Zheng, Y. Huang, X. Zeng, Q. Zhang, Z. Chen, Solvent-free synthesis and hydrophobization of biobased epoxy coatings for anti-icing and anticorrosion applications, ACS Sustain. Chem. Eng. 7 (23) (2019) 19131.
[11] V. Bonamigo Moreira, J. Rintjema, F. Bravo, A.W. Kleij, L. Franco, J. Puiggalí, C. Alemán, E. Armelin, Novel biobased epoxy thermosets and coatings from poly (limonene carbonate) oxide and synthetic hardeners, ACS Sustain. Chem. Eng. 10 (8) (2022) 2708–2719.
[12] J. Ramezanpour, S. Ataei, S.N. Khorasani, Development of smart epoxy coating through click reaction using a vegetable oil, Prog. Org. Coat. 170 (2022), 106985.
[13] Q. Chen, L. Zhang, J. Zhang, S. Habib, G. Lu, J. Dai, X. Liu, Bio-based polybenzoxazines coatings for efficient marine antifouling, Prog. Org. Coat. 174 (2023), 107289.
[14] D.J. Kalita, I. Tarnavchyk, H. Kalita, B.J. Chisholm, D.C. Webster, Bio-based coating resins derived from Cardanol using carbocationic polymerization and their evaluation as one-component alkyd-type coatings, Prog. Org. Coat. 174 (2023), 107252.

[15] Y. Zhang, L. Chu, Z. Dai, N. Bao, M.B. de Rooij, L. Gao, W. Tan, L. Shen, Synergistically enhancing the performance of Cardanol-rich epoxy anticorrosive coatings using Cardanol-based reactive diluent and its functionalized graphene oxide, Prog. Org. Coat. 171 (2022), 107060.
[16] S. Nameer, T. Deltin, P.-E. Sundell, M. Johansson, Bio-based multifunctional fatty acid methyl esters as reactive diluents in coil coatings, Prog. Org. Coat. 136 (2019), 105277.
[17] K. Rajitha, K.N.S. Mohana, A. Mohanan, A.M. Madhusudhana, Evaluation of anti-corrosion performance of modified gelatin-graphene oxide nanocomposite dispersed in epoxy coating on mild steel in saline media, Colloid Surf. A 587 (2020), 124341.
[18] H. Wu, C. Liu, L. Cheng, Y. Yu, H. Zhao, L. Wang, Enhancing the mechanical and tribological properties of epoxy composites via incorporation of reactive bio-based epoxy functionalized graphene oxide, RSC Adv. 10 (66) (2020) 40148–40156.
[19] I. Babahan-Bircan, I. Demirkaya, S.O.H. Hasan, J. Thomas, M.D. Soucek, Comparison of new bio-based epoxide-amine coatings with their nanocomposite coating derivatives (graphene, CNT, and fullerene) as replacements for BPA, Prog. Org. Coat. 165 (2022), 106714.
[20] M. Kosarli, G. Foteinidis, K. Tsirka, D.G. Bekas, A.S. Paipetis, Concurrent recovery of mechanical and electrical properties in nanomodified capsule-based self-healing epoxies, Polymer 227 (2021), 123843.
[21] T. Thakur, B. Gaur, A.S. Singha, Bio-based epoxy/imidoamine encapsulated microcapsules and their application for high performance self-healing coatings, Prog. Org. Coat. 159 (2021), 106436.
[22] H. Wu, J. Li, W. Zhang, T. Chen, F. Liu, E.-H. Han, Supramolecular engineering of nacre-inspired bio-based nanocomposite coatings with exceptional ductility and high-efficient self-repair ability, Chem. Eng. J. 437 (2022), 135405.
[23] X. Wu, F. Yang, G. Lu, X. Zhao, Z. Chen, S. Qian, A breathable and environmentally friendly superhydrophobic coating for anti-condensation applications, Chem. Eng. J. 412 (2021), 128725.
[24] A.C. Balazs, T. Emrick, T.P. Russell, Nanoparticle polymer composites: where two small worlds meet, Science 314 (2006) 1130557.
[25] B.M. Bailey, Y. Leterrier, S. Garcia, S. Van Der Zwaag, V. Michaud, Electrically conductive self-healing polymer composite coatings, Prog. Org. Coat. 85 (2015) 189–198.
[26] R. Ghamsarizade, S. Najafi, A.A. Sarabi, S. Roshan, H.E. Mohammadloo, Synthesis of pH sensitive microcapsules containing ZAPP, SAPP, and 8-HQ, and evaluation of their anti-corrosion performance, and mechanical enhancement of epoxy coating, Prog. Org. Coat. 174 (2023), 107290.
[27] K. Wu, Y. Chen, J. Luo, R. Liu, G. Sun, X. Liu, Preparation of dual-chamber microcapsule by Pickering emulsion for self-healing application with ultra-high healing efficiency, J. Colloid Interface Sci. 600 (2021) 660–669.
[28] S.J. García, H.R. Fischer, S. van der Zwaag, A critical appraisal of the potential of self healing polymeric coatings, Prog. Org. Coat. 72 (2011) 211–221.
[29] D. Sun, Y.B. Chong, K. Chen, J. Yang, Chemically and thermally stable isocyanate microcapsules having good self-healing and self-lubricating performances, Chem. Eng. J. 346 (2018) 289–297.
[30] Z. Yu, A.T.O. Lim, S.L. Kollasch, H.D. Jang, J. Huang, Oil-based self-healing barrier coatings: to flow and not to flow, Adv. Funct. Mater. 30 (2) (2019) 1906273.
[31] S.R. White, N.R. Sottos, P.H. Geubelle, J.S. Moore, M.R. Kessler, S.R. Sriram, E. N. Brown, S. Viswanathan, Autonomic healing of polymer composites, Nature 415 (6873) (2002) 817.
[32] J.D. Rule, E.N. Brown, N.R. Sottos, S.R. White, J.S. Moore, Wax-protected catalyst microspheres for efficient self-healing materials, Adv. Mater. 17 (2005) 205–208.
[33] S. Abbaspoor, A. Ashrafi, R. Abolfarsi, Development of self-healing coatings based on ethyl cellulose micro/nano-capsules, Surf. Eng. 35 (3) (2018) 273–280.
[34] O. Boumezgane, R. Suriano, M. Fedel, C. Tonelli, F. Deflorian, S. Turri, Self-healing epoxy coatings with microencapsulated ionic PDMS oligomers for corrosion protection based on supramolecular acid-base interactions, Prog. Org. Coat. 162 (2022), 106558.
[35] I.O. Arukalam, E.Y. Ishidi, H.C. Obasi, I.O. Madu, O.E. Ezeani, M.M. Owen, Exploitation of natural gum exudates as green fillers in self-healing corrosion-resistant epoxy coatings, J. Polym. Res. 27 (3) (2020) 080.
[36] H. Wang, Q. Zhou, Evaluation and failure analysis of linseed oil encapsulated self-healing anticorrosive coating, Prog. Org. Coat. 118 (2018) 108–115.
[37] J.D. Rule, N.R. Sottos, S.R. White, Effect of microcapsule size on the performance of self-healing polymers, Polymer 48 (2007) 3520–3529.
[38] S.D. Mookhoek, H.R. Fischer, S. van der Zwaag, A numerical study into the effects of elongated capsules on the healing efficiency of liquid-based systems, Comput. Mater. Sci. 47 (2009) 506–511.
[39] S.D. Mookhoek, S.C. Mayo, A.E. Hughes, S.A. Furman, H.R. Fischer, S. van der Zwaag, Applying sem-based x-ray microtomography to observe self-healing in solvent encapsulated thermoplastic materials, Adv. Eng. Mater. 12 (2010) 228–234.
[40] M. Zhang, F. Xu, D. Lin, J. Peng, Y. Zhu, H. Wang, A smart anti-corrosion coating based on triple functional fillers, Chem. Eng. J. 446 (2022), 137078.
[41] G. Peng, Y. Hu, G. Dou, Y. Sun, Y. Huan, S.H. Kang, Z. Piao, Enhanced mechanical properties of epoxy composites embedded with MF/TiO2 hybrid shell microcapsules containing n-octadecane, J. Ind. Eng. Chem. 110 (2022) 414–423.
[42] Z. Bi, F. Gao, M. Liu, R. Zhang, R. Liu, G. Cui, J. Xu, Multifunctional self-healing coatings with orderly distributed microcapsules aligned by magnetic field, Chem. Eng. J. 450 (2022), 138250.
[43] S. Shi, A.N. Netravali, Elongated soy protein isolate-poly(D, L-lactide-co-glycolic acid) microcapsules prepared using syringe filters and their effect on self-healing efficiency of soy protein-based green resin, J. Polym. Environ. 31 (2) (2022) 754–767.
[44] L. Zhou, P. Zhang, L. Shen, L. Chu, J. Wu, Y. Ding, B. Zhong, X. Zhang, N. Bao, Modified graphene oxide/waterborne epoxy composite coating with enhanced corrosion resistance, Prog. Org. Coat. 172 (2022), 107100.
[45] Y.X. Ma, Y.R. Zhang, J.T. Liu, Y.J. Ge, X.N. Yan, Y. Sun, J. Wu, P. Zhang, GO-modified double-walled polyurea microcapsules/epoxy composites for marine anticorrosive self-healing coating, Mater. Des. 189 (2020), 108547.
[46] J. Li, Z. Tao, J. Cui, S. Shen, H. Qiu, Facile fabrication of dual functional graphene oxide microcapsules carrying corrosion inhibitor and encapsulating self-healing agent, Polymers-Basel 14 (2022) 4097.
[47] C. Li, Y. Shi, X. Chen, D. He, L. Shen, N. Bao, Controlled synthesis of graphite oxide: formation process, oxidation kinetics, and optimized conditions, Chem. Eng. Sci. 176 (2018) 319–328.
[48] T. Liu, Z. Zhao, W.W. Tjiu, J. Lv, C. Wei, Preparation and characterization of epoxy nanocomposites containing surface-modified graphene oxide, J. Appl. Polym. Sci. 131 (9) (2014) 40236.
[49] E.N. Brown, S.R. White, N.R. Sottos, Microcapsule induced toughening in a self-healing polymer composite, J. Mater. Sci. 39 (2004) 1703–1710.
[50] S.H. Cho, H.M. Andersson, S.R. White, N.R. Sottos, P.V. Braun, Polydimethylsiloxane-based self-healing materials, Adv. Mater. 18 (8) (2006) 997–1000.
[51] L. Zweifel, C. Brauner, Investigation of the interphase mechanisms and welding behaviour of fast-curing epoxy based composites with co-cured thermoplastic boundary layers, Compos. A Appl. S 139 (2020), 106120.
[52] A.H. Navarchian, N. Najafipoor, F. Ahangaran, Surface-modified poly(methyl methacrylate) microcapsules containing linseed oil for application in self-healing epoxy-based coatings, Prog. Org. Coat. 132 (2019) 288–297.
[53] A.M. Atta, O.E. El-Azabawy, H.S. Ismail, M.A. Hegazy, Novel dispersed magnetite core–shell nanogel polymers as corrosion inhibitors for carbon steel in acidic medium, Corros. Sci. 53 (5) (2011) 1680–1689.